Heliyon 7 (2021) e06674

Contents lists available at ScienceDirect

Heliyon

journal homepage: www.cell.com/heliyon

Research article

Corrosion inhibiting effect of a green formulation based on *Opuntia Dillenii* seed oil for iron in acid rain solution

Malak Rehioui [a,*], Said Abbout [a], Bouchra Benzidia [a], Hind Hammouch [a], Hamid Erramli [a], Naima Ait Daoud [b], Narjis Badrane [b], Najat Hajjaji [a]

[a] *Laboratory of Materials, Electrochemistry and Environment (LMEE), Department of Chemistry, Faculty of Science, Ibn Tofail University, BP 133, 14000, Kenitra, Morocco*

[b] *Anti Poison and Pharmacovigilance Center of Morocco, Ministry of Health, Morocco*

ARTICLE INFO

Keywords:
Opuntia dillenii
Seed oil
Corrosion inhibition
Iron
Acid rain

ABSTRACT

This study examines the development of a new green and eco-friendly formulation derived from *Opuntia dillenii* seed oil (labeled as FOD) and its application as a corrosion inhibitor to protect iron which is subject to corrosion phenomena that become important especially in acidic environments as acid rain.

Physicochemical properties and fatty acid analysis of *Opuntia dillenii* seed oil were performed and they demonstrated that the oil is a major source of unsaturated fatty acids, in particular linoleic acid, with a percentage of 73.388%.

Corrosion inhibition effect of FOD was studied by gravimetric methods, electrochemical measurements, and scanning electron microscopy coupled with elemental analysis (SEM/EDX). Obtained results confirmed that FOD behaves as a good mixed corrosion inhibitor with predominant anodic activity. Inhibition efficiency of FOD is more important when the concentration of FOD and the immersion time increase, reaching values up to 99%. FOD forms a barrier layer on the surface of the iron, and thereby minimizes the contact area between the metal surface and the corrosive solution. The adsorption behavior of FOD on iron surface obeys Langmuir adsorption isotherm with chemisorption and physisorption mechanism.

1. Introduction

Iron is considered one of the most important metals and the most widely used in many industrial applications such as metal construction, building, manufacturing, vehicles, etc. due to its low cost and availability. However, the iron structure is extremely sensitive to corrosion under numerous circumstances, including moisture, corrosive agents and polluted atmosphere [1]. Indeed, the most common issue in iron corrosion resides in its overturning into its chemically stable forms like iron oxide or iron hydride, and thus adversely affects the physicochemical properties of the metals [1].

In addition, corrosion occurs whenever there is an interaction of two different electrochemical reactions on the metal surface. It's a large constant and continuous problem that leads to enormous economic and environmental losses often difficult to eliminate completely [2]. Thus, different techniques are applied to prevent or minimize the corrosion rate of metals and alloys, among which the use of corrosion inhibitor is very popular.

Recently several researches have been performed on the corrosion inhibition including synthetic inhibitors [3, 4, 5, 6] and green inhibitors [7, 8, 9, 10]. In fact, green inhibitors are in urgent need of development because they are environment-friendly, safe and biodegradable. Scientists around the world have been reported the successful use of various natural products and oils extracted from plants as an effective and promising green agent against iron corrosion.

Opuntia dillenii, a succulent plant belonging to the Cactaceae family, commonly known as prickly pear. It's a plant known for its benefits and undeniable features [11, 12]. Indeed, the seeds are used for extracting very valuable vegetable oil which has generated a lot of interest in recent years. Several studies have been carried out to characterize its constituents and in particular to assess its nutritional value as well as their therapeutic effect. In this study, we aimed to investigate the inhibiting effect of a formulation mainly based on *Opuntia dillenii* seed oil (FOD), toward the iron corrosion in the aggressive acid rain atmosphere. Gravimetric method and electrochemical technique such as potentiodynamic polarization, impedance spectroscopy were deployed to examine

* Corresponding author.
E-mail address: rehioui.malak0@gmail.com (M. Rehioui).

https://doi.org/10.1016/j.heliyon.2021.e06674
Received 14 December 2020; Received in revised form 28 February 2021; Accepted 29 March 2021

the inhibition performance. In order to confirm the obtained results, morphological studies of iron electrode surface were performed using scanning electron microscopy SEM coupled with elemental analysis EDX.

2. Experimental study details

2.1. Extraction, physicochemical characteristics and fatty acid analysis of seed oil

Vegetable oil was extracted from *Opuntia dillenii* seeds by the Soxhlet extraction method, according to the recognized ISO 659–1988 method [13]. The solvent used in this process is the cyclohexane.

The physico-chemical characteristics such as density, refractive index, acid index, iodine index, peroxide index, saponification index, and unsaponifiable matter, are determined in accordance with the French Standarization Association [14].

The extracted oil composition was analyzed using gas chromatography Clarus ® 680 (PerkinElmer) coupled with mass spectrometer Clarus ® SQ 8C (PerkinElmer), equipped with a Rxi-5MS capillary column (5% diphenyl, 95% dimethyl polysiloxane), 30 m × 0.25 mm x 0.25 mm. The carrier gas was helium with a flow rate of 1 ml/min. The column temperature initially maintained at 40 °C for 5 min, then ramped at 10 °C/min to 280 °C and held for 10 min. That of the injector was set at 230 °C, with 1 µl injection volume. The operating parameters of the mass spectrometer consist of the temperature source which is 200 °C and the ionized potential (70 eV). The components were identified through their retention times and mass fragmentation models and comparing them with those of the NIST library.

2.2. Corrosion inhibitor, electrode and electrolytic solution

The corrosion inhibitor used in this study was a formulation labelled FOD that mainly based on *Opuntia dillenii* seed oil. The *Opuntia dillenii* plants used were from the region of Essaouira, Morocco, and purchased in a local market in January in Kenitra.

The formulation FOD was prepared according to the process described in the already patented work [15]. The inhibition effect was tested at four different concentrations denoted by, 250, 500, 750 and 1000 ppm.

The electrolyte composition is simulated to acid rain in urban areas near seaside with a high degree of pollution. It consists of 0.2 g/L Na_2SO_4, 0.2 g/L $NaHCO_3$, 0.2 g/L NaCl, and acidified by the addition of sulfuric acid at pH = 3.6 [16].

The material used as the working electrode is iron that was prepared before each experiment by removing the oxide layer on the iron surface by polishing with abrasive papers from 180 to 2000 grades, other organic contaminations and impurities were removed by acetone. Iron chemical composition is given in Table 1 below.

2.3. Gravimetric test

One of the oldest methods used to define the rate of corrosion and the inhibitory efficiency is gravimetry. The amount of iron lost through corrosion is determined either by measuring the weight loss of the metallic iron sample, or by dosing the concentration of dissolved ferric and ferrous ions in solution.

2.3.1. Mass loss measurements

Weight loss measurements were performed using the method previously described [17]. The corrosion rate (ν) and the inhibitor efficiency (IE %) determined according to the following general Eqs. (1) and (2) [18]:

$$\nu = \frac{W}{S\ t} \tag{1}$$

$$IE\ \% = \frac{\nu_0 - \nu}{\nu_0} \times 100 \tag{2}$$

where W is the weight loss (mg), S is the specimen's surface (cm^2), t is the immersion time (24 h), ν_0 and ν are the corrosion rates in absence and presence of inhibitor, respectively (mg cm^{-2} h^{-1}).

2.3.2. Quantification of iron ions by atomic absorption spectrometry

Atomic absorption spectrometry i.e. AAS, model ANALYTIC JENNA NOVA 350, was used to determine the concentrations of dissolved iron in the electrolytic solutions.

This technique allows the measurement of ferrous and ferric ions dissolved in solution during 24 h of immersion without and with various concentrations of inhibitor.

2.4. Electrochemical methods

In order to examine the approach of mechanisms and phenomena involved during the corrosion, electrochemical techniques have been employed to define instantaneous corrosion rates and to elucidate the influence of the inhibitor on the mechanisms of the iron corrosion process.

All electrochemical experiments were conducted using Potentiostat/Galvanostat type Bio-logic SP-200 with a conventional three-electrode cell consisting of a platinum electrode as counter electrode, a saturated calomel electrode (SCE) as reference electrode, and an iron working electrode.

Open circuit potential (OCP) monitoring was performed through immersing the working electrode in the corrosive solution in absence and presence of inhibitor during 30 min.

The potentiodynamic polarization curves (PPC) were performed on iron electrode by automatically changing the electrode potential from -1.0 to -0.2 V (vs. SCE) using a scan rate of 1 mV s^{-1}, after automatic ohmic drop compensation (ZIR). The electrochemical parameters (i_{corr}, E_{corr}, βa and βc) are determined by the EC-Lab software. Inhibitory efficiency was calculated from the following formula (3) [17, 18, 19]:

$$IE(\%) = \frac{i_{corr0} - i_{corr}}{i_{corr0}} \times 100 \tag{3}$$

where, i_{corr0} and i_{corr} are the corrosion current densities in absence and presence of FOD, respectively.

Electrochemical impedance spectroscopy (EIS) measurements were performed by applying a signal amplitude perturbation of 10 mV, in the frequency range of 100 kHz to 10 mHz. The recorded of EIC spectra begins after 30 min of immersion. Then, the impedance data were examined with the aid of EC-LAB software and the results were typically fitted to a suitable equivalent electrical circuit. The inhibitory efficiency was calculated according to Eq. (4) [17, 18, 19]:

$$IE\ (\%) = \frac{R_P - R_{P0}}{R_P} \times 100 \tag{4}$$

where R_{p0} and R_p represent the polarization resistances values in absence and presence of FOD, respectively.

All electrochemical measurements were performed at least three times to ensure the reliability of the results.

2.5. Surface characterization by SEM/EDX

Surface morphology of iron samples was characterized before and after exposure in the corrosive solution during 24 h and in presence of inhibitor using a scanning electron microscope (Quattro ESEM), with an acceleration voltage of 20 kV and a working distance of 8 mm. Meanwhile, the elemental constituents of iron were recorded using an Energy Dispersive X-Ray Spectroscopy.

Table 1. Chemical composition of the iron sample.

Element	Si	Mn	C	P	S	Fe
Wt (%)	0.2	0.519	0.157	0.007	0.009	≥ 99%

3. Results and discussion

3.1. Physicochemical characteristics and fatty acid profile

The maximum yield of oil extracted from *Opuntia dillenii* seeds is 10.63%. It is achieved after 10 h of extraction by the Soxhlet apparatus. The Physicochemical characteristics provide more information about the purity and quality of the oil studied (Table 2).

As shown in Table 2, the density value of *Opuntia dillenii* seed oil was 0.929. The refractive index of oils depends on their molecular weight, fatty acid chain length, degree of unsaturation, and degree of conjugation. The refractive index of *Opuntia dillenii* seed oil was 1.441. The iodine value was approximately 121.82 g/100 g; this high value indicated a high degree of unsaturation of the oil.

The peroxide value is an index of rancidity, thus the high peroxide value of oil indicates a poor resistance of the oil to peroxidation during storage. The peroxide value of *Opuntia dillenii* seed oil was 5.31 meq O_2/kg of oil, which is bellow the maximum acceptable value of 10 meq.O_2/kg set by Codex Alimentarius Committee [20]. The acid value of the oil was 5.75 mg of KOH/g. This low value was a result of lower hydrolysis of triglycerides. *Opuntia dilleniii* seed oil had a saponification value of 175.31 mg KOH/g, which indicates a high content of medium chain fatty acids (i.e. C18 and C16).

Previous research presented by Ghazi revealed a density of 0.895, a refractive index of 1.4728, an acid value of 1.14 mg of KOH/g, and a saponification value of 180 mg KOH/g [21]. The difference between the results may be due to the difference in the growth region and the degree of maturity, also to the difference in the extraction method, because Ghazi had extracted the *Opuntia dillenii* seed oil by the maceration method.

Oil chemical composition determined by GC/MS, is reported in Table 3.

As illustrated in Table 3, it is found that linoleic acid is the dominating fatty acid with an exceptional level up to 73.388%, followed by palmitic acid 16.332% and stearic acid 3.67%. Whereas, oleic and myristic acids are detected with a small proportion. These results demonstrated that the oil is highly unsaturated since it is composed of 75.059% of unsaturated fatty acids.

For the same study, the results obtained by Ghazi et al. [22] are almost similar: linoleic acid (79.83%), palmitic acid (13.52%) and stearic acid (2.75%). Alsaad et al. [23] revealed also that the main fatty acids contained in this oil were linoleic acid (72.9%), palmitic acid (15.12%) and stearic acid (7.51%). On the other hand, Liu et al. [24] reported that linolenic acid was the main fatty acid (66.56%), followed by palmitic acid (19.78%), stearic acid (9.01%) and linoleic acid (2.65%). The observed difference is probably due to the degree of maturity of the fruit or to the harvesting area characteristics.

Table 2. Physicochemical characteristics of *Opuntia dillenii* seed oil.

Physico-chemical characteristics	Value (mean ± Deviation)
Density at 20 °C	0.929 ± 0.034
Refractive index at 20 °C	1.441 ± 0.002
Iodine index (g/100g)	121.82 ± 0.25
Acid index (mg $_{KOH}$/g)	5.75 ± 0.07
Peroxide value (meq$_{O2}$/Kg $_{Oil}$)	5.31 ± 0.03
Saponification index (mg $_{KOH}$/g)	175.31 ± 1.94
Unsaponifiable matter %	1.25 ± 0.02

Otherwise, this oil contains also an amount of the sterolic fraction which is composed of γ-sitosterol 2.211%, Campesterol 0.912%, and Stigmasterol 0.855%. The γ-tocopherol as a major form of vitamin E is present in an amount of 0.674%.

3.2. Gravimetric study

Iron samples weight loss was studied without and with different concentrations of FOD in the corrosive solution (acid rain solution) after 24 h immersion time at room temperature. The corrosion rate (ν) and inhibition efficiency (% IE) values are listed in Table 4.

The results demonstrated that iron was severely corroded in the uninhibited acid rain solution, whereas the presence of inhibitor reduced iron dissolution rate considerably, due to the interaction of inhibitory molecules with the iron surface. The protection efficiency increases, with the increase of FOD concentration, and reaches a maximum value of 94.34% at 1000 ppm of inhibitor, which shows the excellent inhibitory property of FOD against iron corrosion in acid rain solution.

The results obtained from quantification of ferrous and ferric iron ions by the atomic absorption spectrometry technique are tabulated in Table 5.

It's noted from this table that dissolved iron ions in solution decrease with the increase of FOD concentration, this can be explained by the protection of the iron substrate by an inhibiting film formed. The maximum inhibition efficiency about 93% was obtained at a concentration of 1000 ppm of inhibitor. This outcome is in agreement with that obtained by weight loss measurement.

3.3. Electrochemical measurements

3.3.1. Open circuit potential (OCP)

Figure 1 depicts the variation of OCP of iron as a function of time measured in acid rain free of inhibitor and with different concentrations of FOD.

It can be seen that the potential for blank test tends to stabilize at -0.55 V/SCE. This observation explains the corrosion reactions on iron surface under this corrosive environment and the formation of corrosion products.

When the tests are conducted in the presence of 250, 500 or 750 ppm of FOD, the corrosion potential E_{corr} shifted rapidly toward less negative values during the first seconds, then continued to head to more positive direction until stabilization. This shift suggests that FOD affected the anodic reaction [25].

After adding 1000 ppm of FOD, E_{corr} shifted for the first few seconds to more negative values, and then shifted to positive direction but below the curve of 750 ppm. The inhibitor seems to act by reducing the active surface without changing the mechanism, except for 1000ppm. This is why we noted this difference. This will be confirmed by the results of the potentiodynamic polarization curves.

However, the displacement of Ecorr to the positive direction suggests that FOD has influenced the anodic reaction and can delay the anodic reaction of iron dissolution due to the formation of a protective layer of the inhibitor on the iron surface [25].

3.3.2. Potentiodynamic polarization curves (PPC)

Tafel polarization plots obtained for the iron in the corrosive medium without and with various concentrations of FOD are presented in Figure 2.

In the absence of the inhibitor, the corrosion potential E_{corr} is -499.082 mV/SCE, a low value that shows the active state of corrosion. The cathodic curve is distinguished by a current plateau may be imputed to the oxygen diffusion process, denoting the importance of mass transport factor that had to be considered in the cathodic process [26]. The corresponding reaction in the aerated acid rain solution at pH = 3.6 is expressed by Eq. (5) [26, 27]:

Table 3. Chemical composition of *Opuntia dillenii* seed oil.

Chemical composition		Concentration (%)
Fatty acids	Palmitic $C_{16:0}$	16.332
	Linoleic $C_{18:2}$	73.388
	Stearic $C_{18:0}$	3.267
	Oleic $C_{18:1}$	1.671
	Myristic $C_{14:0}$	0.681
Sterols	γ - sitosterol	2.211
	Campesterol	0.912
	Stigmasterol	0.855
Vitamine E	γ-tocopherol	0.674

Table 4. Corrosion rate and inhibitory efficiency of FOD.

FOD concentration (ppm)	ν (mg.cm^{-2}.h^{-1})	IE (%)
0 (acid rain)	0.247 ± 0.084	—
250	0.030 ± 0.035	87.85 ± 0.04
500	0.022 ± 0.026	91.10 ± 0.02
750	0.018 ± 0.029	92.72 ± 0.03
1000	0.014 ± 0.019	94.34 ± 0.02

$$O_2 + 4H^+ + 4e^- \rightarrow 2H_2O \quad (5)$$

The effect of hydrogen reduction is also taken into account, according to the following reaction (6):

$$2H^+ + 2e^- \rightarrow H_2 \quad (6)$$

In the anodic section, a rapid increase of the current density value was observed. The corresponding anodic oxidation reaction that is attributed to the iron dissolution is expressed by Eq. (7):

$$Fe \rightarrow Fe^{2+} + 2e^- \quad (7)$$

The addition of FOD has shifted the corrosion potential E_{corr} to positive direction. Besides, the presence of FOD affects both cathodic and anodic behavior. In the cathodic branch, we noticed the decrease in the cathodic current densities values, and we highlighted the disappearance of the diffusion plateau obtained in the case of the corrosive solution without inhibitor; which is due to the formation of an inhibitor layer on the metal surface that hinders the diffusion of dissolved oxygen towards the electrode surface.

Regarding the anodic branch, the curves registered a decrease in the value of the anodic current densities, with a change in the shape of the curves indicating a change in the corrosion mechanism. At the addition of 500 ppm or 750 ppm in FOD, the anodic current density is limited to the vicinity of the corrosion potential indicating the start of film formation on the metal surface, but at high potentials, the anodic current densities have increased rapidly. This can be correlated to the breakdown of the inhibitor formed film.

However at 1000 ppm in FOD, we noticed a current plateau in a wide range of potential. Thus, the corresponding current density values are very low values compared to those of the corrosive solution without FOD.

Table 5. Dissolved iron concentration and inhibition efficiency determined by AAS method.

FOD concentration (ppm)	Dissolved Fe (mg/L)	IE (%)
0 (acid rain)	7.148	—
250	0.878	87.92
500	0.601	90.69
750	0.587	91.96
1000	0.510	93.01

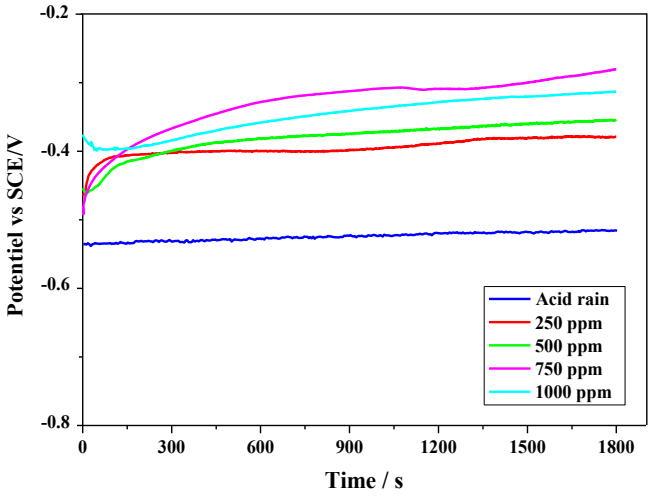

Figure 1. Variation of the open circuit potential of iron in acid rain solution at different concentrations of the inhibitor.

This is attributed to the passivity of iron, resulting from the formation of a passive inhibitor film on the metal surface, which indicates that the metal surface is well protected.

Table 6 summarizes the kinetic parameters determined by extrapolation of the polarization curves using the EC-Lab software, the corrosion current density (i_{corr}), the corrosion potential (E_{corr}), the cathodic βc and anodic βa Tafel slopes, as well as the corrosion inhibitory efficiency IE (%).

The results collected in Table 6 indicated a decrease in the current density values from 78.33 μA/cm^2 to 1.27 μA/cm^2, and therefore an increase in the inhibitory efficiency, attaining 98.37% at 1000 ppm, which confirms better protection of FOD against iron corrosion in the simulated acid rain solution.

These results allowed us to conclude that FOD can be classified as mixed-style inhibitor. Thus FOD not only inhibited the anodic metal dissolution reaction, but also controlled the cathodic oxygen absorption reaction [28]. However, it was reported that if the displacement in corrosion potential is more than ±85 mV with respect to the corrosion potential of the blank, the inhibitor can be considered as a cathodic or anodic type [29]. The maximum displacement in the present study is more than 149 mV, was moved towards the anode direction, reflecting the dominance of the anodic inhibitor type. This excellent protective effect of FOD can be related to its adsorption through the oil molecules on the iron surface and to the formation of a film which constitutes an

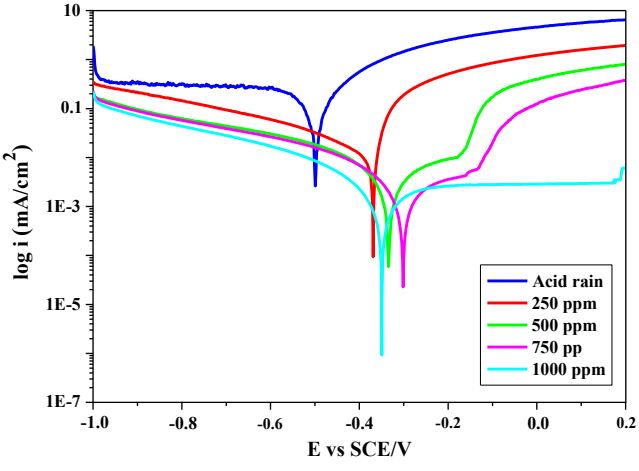

Figure 2. Potentiodynamic polarization plots recorded for iron in acid rain without and with different FOD concentrations.

adherent barrier between the surface of the iron substrate and the corrosive medium.

Similar behaviors and phenomena have been observed in previous research projected by Chellouli and al [10]. that developed a formulation based on *Nigella Sativa* seeds oil (FBN) against iron corrosion in acid rain medium. The similarity in the results may be due to the chemical composition of the oils. *Nigella Sativa* seed oil was mainly composed of linoleic acid (55.84%), oleic acid (22.70%), palmitic acid (12.32%), stearic acid (3.35%) and linolenic acid (0.59%) [30]. Compared to that of *Opuntia Dillenii*, which consisted predominantly of linoleic acid with a level reaching 73.388% followed by palmitic acid 16.332%, stearic acid 3.267%, oleic acid 1.671% and myristic acid 0.681%. Both oils are highly unsaturated since the seed oil of *Nigella Sativa* is composed of 79.13% unsaturated fatty acids. While that of *Opuntia Dillenii* consists of 75.059%. It is noted that the dominant fatty acid in both oils is linoleic acid.

To find out which ingredient is responsible for inhibiting iron corrosion in acid rain solution, we decided to conduct a study on the combination of both oils in one formulation labeled FNOD to protect iron against acid rain corrosion. FNOD is relied on the preparation of a concentration of 1000 ppm that combines 50% *Opuntia Dillenii* seed oil and 50% *Nigella Sativa* seed oil (50/50, v/v). Figure 3 represent the polarization curves of iron in the acid rain medium in the presence of 1000 ppm of FOD, FBN and the new formulation FNOD. The electrochemical parameters deduced from these curves are presented in Table 7.

In general, the adsorption depends on the carboxylic group and the unsaturation of fatty acids. The greater fatty acids have π bonds in their carbon chains, the greater the possibility of sharing the π electrons with vacant d orbitals of iron, and therefore the greater the absorption of fatty acids at iron surface, creating a layer addressing the declination of corrosion [31, 32]. To see the influence of fatty acids on adsorption, as can be seen from Table 7, the corrosion efficiency of FNOD (99.10%) is almost the same as FBN (98.98%). However it is slightly greater than that of FOD (98.37%). The small difference is due to the influence of unsaturated fatty acids, because there is a difference of 4.071% of unsaturated fatty acids between *Nigella Sativa* seed oil which is composed of 79.13% usaturated fatty acids and the *Opuntia Dillenii* seed oil which is composed of 75.059% unsaturated fatty acids [30].

3.3.3. Electrochemical impedance spectroscopy (EIS)

Electrochemical impedance spectroscopy (EIS) is one of the best powerful analytical tools in electrochemistry. It's allowed us to analyze the properties of the electrochemical systems [33]. The obtained EIS spectra are shown in Figure 4.

As can be seen from Figure 4, the curve in the case of the acid rain solution without inhibitor exhibited two capacitive non-ideal semicircle loops at high and low frequencies, and a small inductive loop at very low frequencies. The inductive loop may be attributed to the relaxation of adsorbed species presents in the corrosive solution, or to the re-dissolution of the passivity surface [10, 34]. Nevertheless, the shape of the curve was affected after addition of the inhibitor FOD, the inductive loop was disappeared, and also the diameter of the capacitive loops grows according to the increase in FOD concentration. Increasing in the size of the loops indicates the ability of FOD to act at the electrolyte/surface interface and generate iron protection.

The equivalent electrical circuits used to model iron/solution interface for these systems are presented in Figure 5.

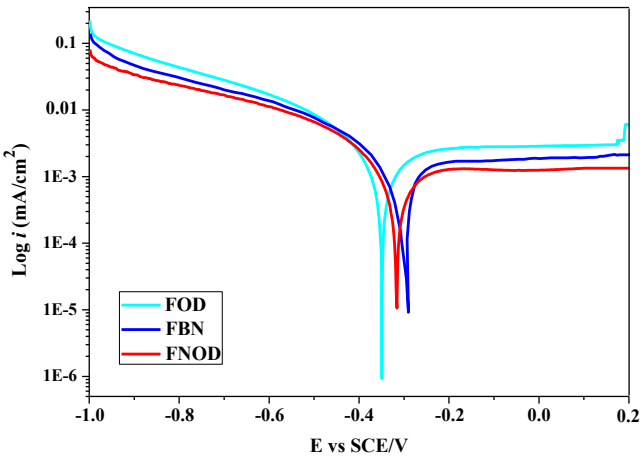

Figure 3. Potentiodynamic polarization plot.

The equivalent electrical circuit consists in the absence of inhibitor of electrolytic resistor *Re*; resistors in high and low frequencies which are respectively R_{HF} and R_{BF} and inductance *L* (Figure 5a).

However, in the presence of inhibitor, the circuit showed the absence of inductive element in the impedance spectrum. While R_f represents the film resistance, its evolution is related to the increase of the protective power of the film or the electrolyte penetration through the film. C_f represents the film capacity related to the dielectric character. R_t is the charge transfer resistor. C_{dl} is the double layer capacity at the electrolyte/iron interface at the bottom of the pores [35, 36] (Figure 5b).

The fitting parameters relating to equivalent circuits are listed in Tables 8a and 8b.

Tables 8a and 8b obviously showed the increase of the values of the charge transfer resistances R_t and the film resistances R_f as a function of the inhibitor concentration. Conversely, the values of the film capacities C_f have decreased with the increase in FOD concentration ($C_f < 10$ μF/cm^2), which is probably attributed to the formation of a protective layer on the electrode surface [7, 26]. The reduction of the double layer capacitance C_{dl} values might be explained by the decrease in the surface heterogeneity. Otherwise there is a decrease in the electrolyte resistance after adding the inhibitor which may indicate that the solution is charged with ionized elements of the formulation [37].

The adsorption of the inhibitor molecules on the surface of the iron electrode causes the formation of a protective layer between the metal and the corrosive medium ions [38]. The same behavior has been observed in several research studies concerning the same medium [9, 10, 26, 34]. The inhibitory efficiency reaches a value of 99.19% for a concentration of 1000 ppm of the inhibitor. This result is in good agreement with those obtained from stationary electrochemical measurements and gravimetric measurements.

3.4. Effect of immersion time

Monitoring the influence of the immersion time of iron corrosion in the aggressive medium provides important information on the stability of the protective layer formed on the metal surface.

Table 6. Kinetic parameters for acid rain and FOD inhibitor derived from polarization curves.

Concentration of inhibitor (ppm)	E_{corr} (mV/SCE)	i_{corr} (μA/cm^2)	- βc (mV/dec)	βa (mV/dec)	IE (%)
0 ppm (Acid rain)	-499.08 ± 0.90	78.33 ± 0.19	353.1 ± 0.6	104.8 ± 0.3	—
250	-368.66 ± 0.61	9.92 ± 0.10	188.3 ± 0.5	139.7 ± 0.3	87.33 ± 0.9
500	-334.23 ± 0.40	2.99 ± 0.05	176.0 ± 0.4	250.1 ± 0.4	96.18 ± 0.9
750	-301.48 ± 0.47	1.87 ± 0.02	172.7 ± 0.3	322.5 ± 0.5	97.61 ± 0.08
1000	-349.33 ± 0.42	1.27 ± 0.02	166.2 ± 0.3	398.7 ± 0.6	98.37 ± 0.08

Table 7. Kinetic parameters derived from polarization curves.

Inhibitor	Concentration (ppm)	E_{corr} (mV/SCE)	i_{corr} (μA/cm^2)	-βc (mV/dec)	βa (mV/dec)	IE (%)
FOD	1000	-349.33 ± 0.42	1.27 ± 0.03	166.2 ± 0.3	398.7 ± 0.6	98.37 ± 0.08
FBN	1000	-287.82 ± 1.11	0.80 ± 0.03	201.1 ± 0.5	301.7 ± 0.7	98.98 ± 0.08
FNOD	1000	-315.75 ± 1.08	0.70 ± 0.02	183.1 ± 0.8	341.4 ± 0.8	99.10 ± 0.07

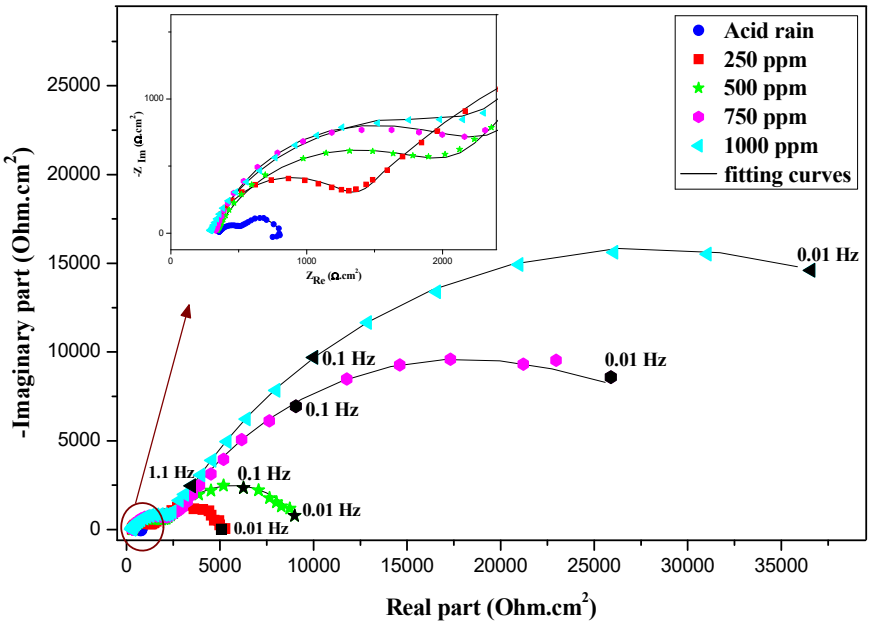

Figure 4. Nyquist plots recorded for iron in acid rain solution with and without inhibitor.

For longer immersion times, modifications of the formed inhibitor film could be characterized by impedance spectroscopy. Indeed, Figure 6 proves the impedance diagrams obtained during iron corrosion tests in a simulated acid rain environment in the presence of 1000 ppm of inhibitor conducted over 120 h.

As time lapse, the electrochemical impedance diagrams reveal an increase in the impedance plots, which is attributed to the improvement of the layer formed on the iron surface and its densification.

However we are seeing a slight change in the shape of the diagrams obtained. The low frequency loop becomes more linear and severe, and begins to overlap with the high frequency loop for a longer immersion time, the polarization resistance R_p tends towards very large values. This behavior may be ensues from Warburg impedance, which represented the diffusion process through the formed inhibitor film on the interface of metal, resulting in linear slope increase with the increase of immersion time [39, 40]. This could occur because the FOD absorbed on the metal surface forms a monolayer, and the high immersion time makes the inhibitor film porous, and thus the process of ions diffusion through the pores of the inhibitor films increased with increasing immersion time, resulting in a porous surface.

3.5. Adsorption isotherm

Adsorption isotherms are used to investigate the nature of interaction of inhibitor molecules on metal surface. Several adsorption models have been attempted for fitting the adsorption of FOD inhibitor on iron surface in acid rain. Langmuir adsorption isotherm was found to be the best fit. The mathematical expression of the Langmuir isotherm is given by Eq. (8) [41]:

$$\frac{C}{\theta} = \frac{1}{K_{ads}} + C \tag{8}$$

where C is the inhibitor concentration, K_{ads} is the adsorption equilibrium constant, and θ is the surface coverage. θ could be defined as θ = EI (%)/100. The plot of C/θ versus C yielded a straight line with a slope close to 1 at the different electrochemical techniques (EIS and PPC), as shown in Figure 7. It clearly reveals that the adsorption of FOD on the iron surface obeys the Langmuir isotherm. The standard Gibbs free energy of adsorption ΔG°_{ads} can be determined according to Eq. (9):

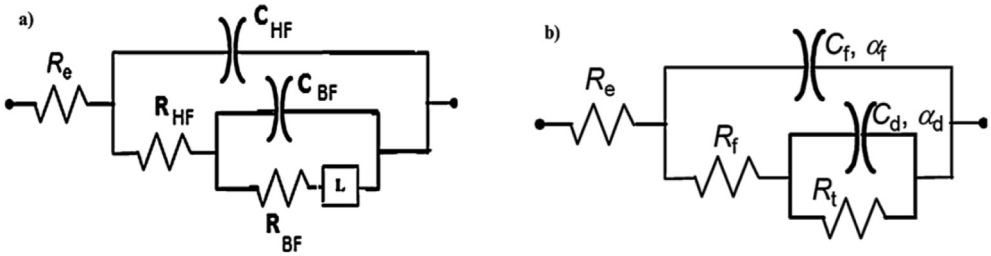

Figure 5. Scheme of the equivalent electric circuits (EEC) used for iron in acidic solution in the absence (a) and the presence (b) of the FOD formulation.

Table 8a. Electrochemical parameters associated with the EIS diagram of acid rain solution.

	R_e (Ω.cm^2)	R_{HF} (Ω.cm^2)	C_{HF} (μF/cm^2)	R_{BF} (Ω.cm^2)	C_{BF} (μF/cm^2)	R_p (Ω.cm^2)
Acid rain	356 ± 2.1	183 ± 1.8	58.01 ± 0.09	255 ± 1.8	572.98 ± 1.35	438 ± 1.2

Table 8b. Electrochemical parameters associated with the EIS diagrams in presence of various concentrations of FOD formulation.

FOD concentration (ppm)	R_e (Ω.cm^2)	R_f (Ω.cm^2)	C_f (μF/cm^2)	R_t (Ω.cm^2)	C_{dl} (μF/cm^2)	R_p (Ω.cm^2)	IE (%)
250	310 ± 1.5	1 101 ± 2.2	1.50 ± 0.09	3 800 ± 4.5	179.76 ± 0.98	4 901 ± 2	91.06 ± 0.13
500	328 ± 1.3	1 963 ± 3.3	1.37 ± 0.05	7 214 ± 3.8	170.14 ± 1.38	9 177 ± 2.3	95.23 ± 0.12
750	323 ± 0.9	2 142 ± 3.5	0.82 ± 0.06	31 015 ± 8.2	159.67 ± 1.18	33 157 ± 7.2	98.68 ± 0.18
1000	284 ± 1.1	2 343 ± 4	0.79 ± 0.01	51 638 ± 8.3	153.22 ± 1.48	53 981 ± 7	99.19 ± 0.14

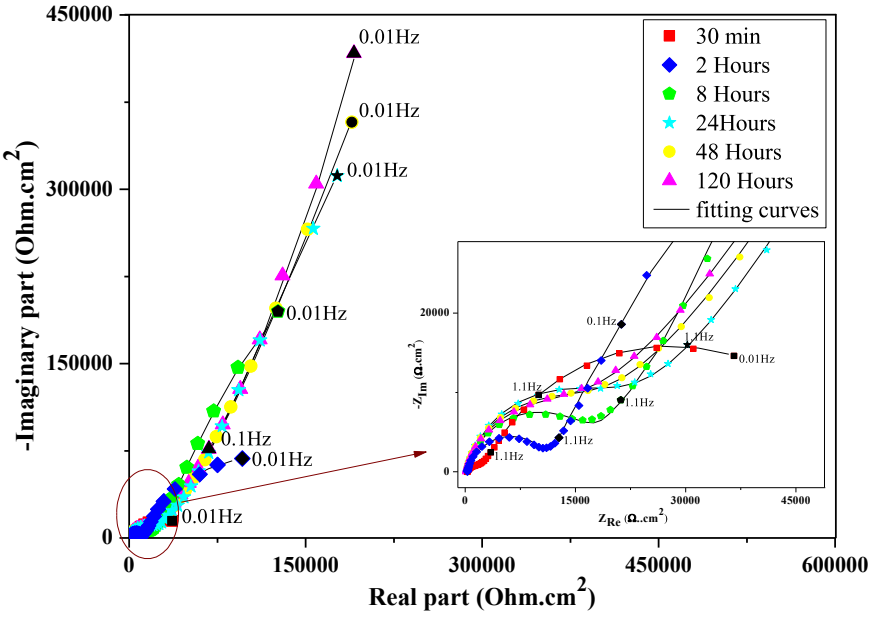

Figure 6. EIS spectra of the iron electrode in the acid rain solution containing 1000 ppm of the formulation at different immersion times.

$$\Delta G^{\circ}_{ads} = -RT\,Ln(1000 \times K_{ads}) \quad (9)$$

where 1000 is the mass concentration of water in solution, R and T denote universal gas constant, and temperature in Kelvin scale respectively.

Thermodynamic parameters are calculated and listed in Table 9. According to literature, ΔG°_{ads} value around -20 kJ/mol or less negative implies an electrostatic interaction between charged inhibitor molecules and charged metal surface which called physisorption. While those around -40 kJ/mol or more negative involve charge sharing or transfer from inhibitor molecules to metal surface to enhance the formation of a coordinate covalent bonds which is named chemisorption [31, 41]. From Table 9, the negative values of the magnitudes ΔG°_{ads} indicate the spontaneous adsorption of the inhibitor on the iron surface. In addition, the values lie between -20 and -40 kJ/mol (-25.218 kJ/mol for PPC and -25.568 kJ/mol for EIS), which likely mean that the plausible inhibition mechanism of FOD was explained by both physical and chemical forces [41].

However, the inhibitive properties of the adsorbed layer on the iron surface would considerably depend on the fatty acid molecules present in *Opuntia dillenii* seed oil. Chemical adsorption of fatty acids might occur due to interactions between the unshared electron pairs in oxygen atoms of the head group with vacant d orbitals of the iron atoms to give a protective chemisorbed film. Moreover, the presence of double bonds in

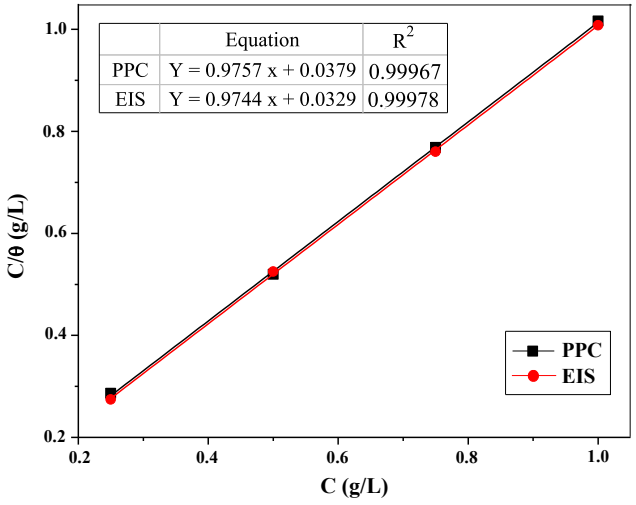

Figure 7. Langmuir isotherm for adsorption of FOD on iron surface in acid rain solution.

Table 9. Thermodynamic parameters of inhibitor adsorption calculated using different electrochemical studies results.

	Slope	K_{ads} (L/mol)	ΔG°_{ads}(KJ/mol)	R^2
PPC	0.9757 ± 0.0102	26.3296 ± 0.0112	-25.218 ± 0.020	0.99967 ± 0.00006
EIS	0.9744 ± 0.0083	30.3306 ± 0.0081	-25.568 ± 0.009	0.99978 ± 0.00004

fatty acids could also share the localized π electrons with iron d orbitals. Otherwise, physical adsorption could results from the electrostatic binding of the active functional group in fatty acids (carboxylate anion $-COO^-$) with the positively charged iron surface [31, 32].

3.6. Surface analysis

3.6.1. Scanning electron microscopy

To confirm the results obtained previously, qualitative microscopic analyses of SEM were performed. Figure 8 shows the surface states of iron samples before and after 24 h of immersion in acid rain solution as well as in presence of FOD or FNOD. For comparison, the iron morphology before immersion (control sample), shown in Figure 8a, is very smooth and shows no corrosion excluding some minor micro-cracks due to polishing. While the image of the surface exposed to acid rain solution (Figure 8b) is strongly damaged by the medium and covered by corrosion products.

However, in the presence of FOD (Figure 8c) the attack is less observed. It's also revealed the formation of a less uniform inhibitor layer, which further confirms the inhibition action of FOD. In the presence of FNOD (Figure 8d), the iron surface is notably improved, considering its flatness and smoothness, indicating an improvement in the protective film formed on the metallic surface.

3.6.2. Energy dispersive X-ray spectroscopy

Figure 9 illustrates the corresponding EDX spectra. As we can see, the surface of the control sample (Figure 9a) contains the specific elements peaks corresponding to the studied iron sample. In acid rain solution without inhibitor (Figure 9b), the EDX spectrum detects the appearance of a high oxygen content on this sample as well as small peaks of the atoms of chlorine and sulfur. This may indicates the presence of iron oxides (FeO, Fe_2O_3), hydroxides species (FeOOH) or sulphates compounds ($Fe_2(SO_4)_3$) over the iron surface.

Whereas, in the presence of FOD (Figure 9c), the EDX spectrum shows the decrease in oxygen peak, the disappearance of chlorine and sulfur peaks and the increase in the carbon peak. This undoubtedly indicates the presence of FOD molecules on the iron surface that block its damages and preclude the formation of corrosion compounds through its strong adsorption on the surface. On the other hand, the appearance of a small peak of silicon may be due to contamination during experiments. We observe the same when we add FNOD to the blank solution (Figure 9d), the decrease in the oxygen peak and the increase in the carbon peak, indicating the adsorption of inhibitory molecules to the iron surface and justifying the inhibitory role of the formulation FNOD.

SEM and EDX analysis confirms the promising performances obtained by electrochemical measurement and can explain the high efficiency values.

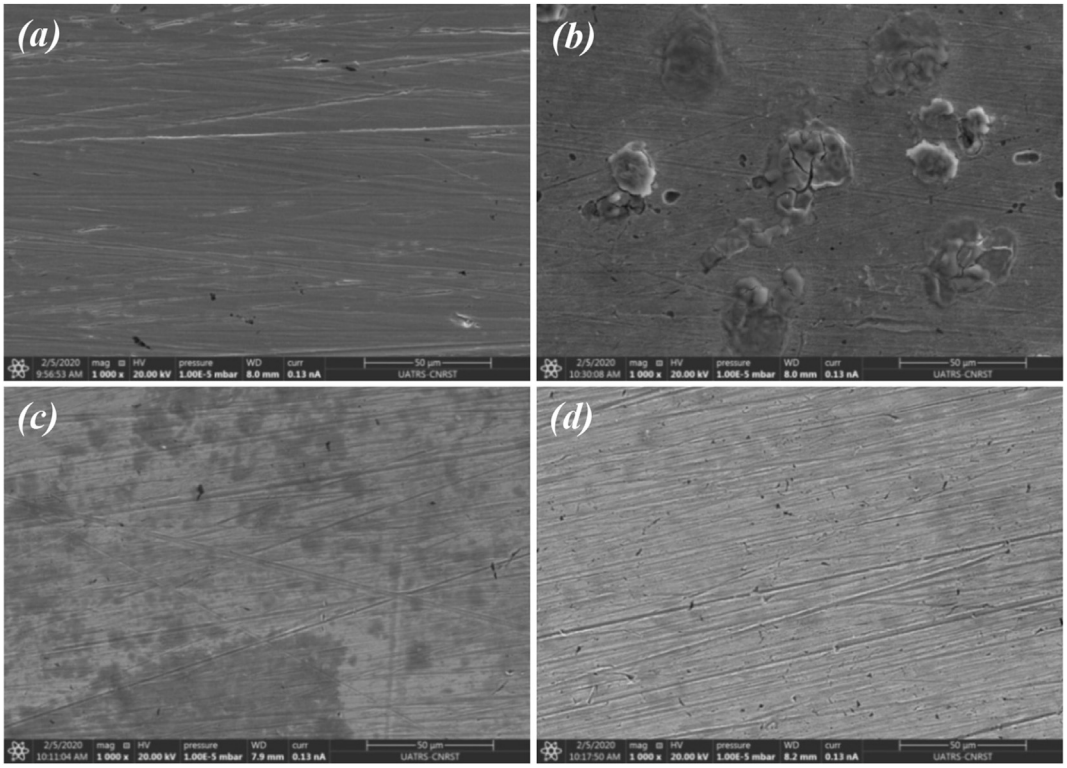

Figure 8. SEM images of iron before (a) and after 24 h of immersion in acid rain solution (b), and in the presence of 1000 ppm of FOD (c) or 1000 ppm of FNOD (d).

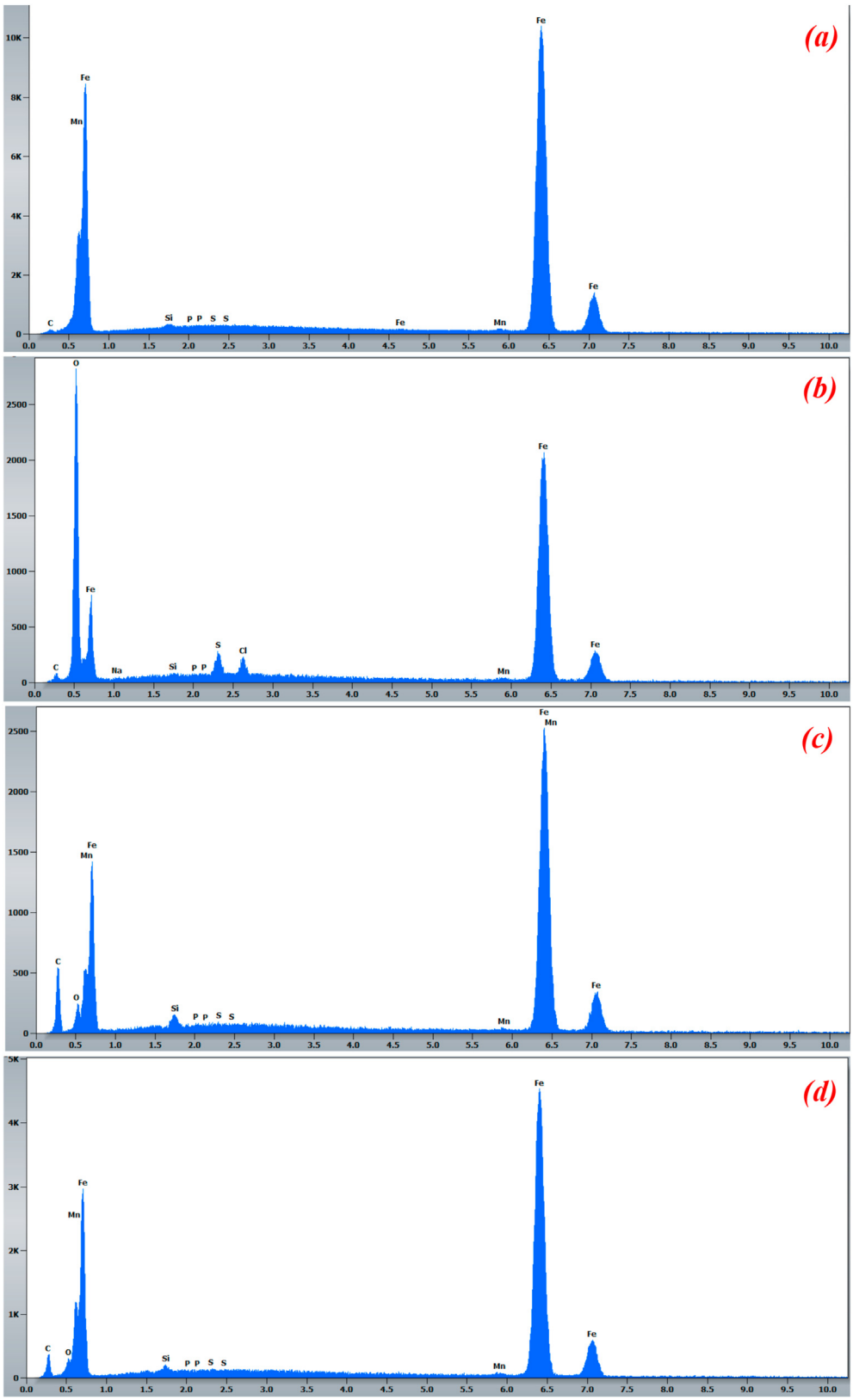

Figure 9. EDX spectra of the iron surface before (a) and after 24h of immersion in the acid rain solution (b), and in the presence of 1000 ppm of FOD (c) or 1000 ppm of FNOD (d).

4. Conclusion

This research demonstrated the feasibility and the potential of a formulation based on *Opuntia dillenii* seed oil (FOD) to inhibit iron corrosion in acidic rain solution. The results allowed us to draw the following conclusions:

- Physicochemical characteristics and fatty acid analysis have shown that *Opuntia dillenii* seed oil is a major source of unsaturated fatty acids.
- Achievements from the potentiodynamic polarization plots demonstrated that FOD can effectively reduce the corrosion current density as a function of the concentration, indicating the mixed type protection character with an anodic predominance.
- The FNOD formulation that combines *Opuntia Dillenii* seed oil and *Nigella Sativa* seed oil in equal parts indicated the same behavior and results deducted from the polarization plot, proving that the inhibition efficiency is mainly due to the influence of unsaturated fatty acids.
- The EIS plots were affected by the two studied variables, the sizes of the loops increased with the increase in the inhibitor concentration and the increase in the immersion time.
- The good inhibitory effect of FOD is attributed to the formation of a protective barrier composed of FOD molecules on the metal surface.
- Adsorption of FOD on iron surface obeys Langmuir adsorption isotherm with chemisorption and physisorption mechanism.
- The surface morphology study by SEM coupled with EDX confirms the high protective effect of FOD by the formation of an inhibitor film on the metal surface which limits the corrosion rate due to the acid rain solution.
- The data obtained from the different methods (gravimetric, potentodynamic polarization, EIS and SEM/EDX) were in good agreement.

Declarations

Author contribution statement

Malak Rehioui: Conceived and designed the experiments; Performed the experiments; Analyzed and interpreted the data; Wrote the paper.

Said Abbout, Bouchra Benzidia: Performed the experiments; Analyzed and interpreted the data.

Hind Hammouch, Hamid Erramli: Analyzed and interpreted the data.

Naima Ait Daoud, Narjis Badrane: contributed reagents, materials, analysis tools or data.

Najat Hajjaji: Conceived and designed the experiments; Analyzed and interpreted the data.

Funding statement

This research did not receive any specific grant from funding agencies in the public, commercial, or not-for-profit sectors.

Data availability statement

Data included in article/supplementary material/referenced in article.

Declarations of interest statement

The authors declare no conflict of interest.

Additional information

No additional information is available for this paper.

References

[1] H. Seddiqi, A. Sadatshojaie, B. Vaferi, E. Yahyazadeh, A. Salehi, D.A. Wood, Mathematical model for Iron corrosion that eliminates chemical potential parameters, Chin. J. Chem. Eng. 28 (2019) 603–612.
[2] I.A. Adejoro, F.K. Ojo, S.K. Obafemi, Corrosion inhibition potentials of ampicillin for mild steel in hydrochloric acid solution, J Taibah Univ Sci 9 (2015) 196–202.
[3] A. Chaouiki, H. Lgaz, Ill-Min Chung, I.H. Ali, S.L. Gaonkar, K.S. Bhat, R. Salghi, H. Oudda, M.I. Khan, Understanding corrosion inhibition of mild steel in acid medium by new benzonitriles: insights from experimental and computational studies, J. Mol. Liq. 266 (2018) 603–616.
[4] R. Hsissou, B. Benzidia, M. Rehioui, M. Berradi, A. Berisha, M. Assouag, N. Hajjaji, A. Elharfi, Anticorrosive property of hexafunctional epoxy polymer HGTMDAE for E24 carbon steel corrosion in 1.0 M HCl: gravimetric, electrochemical, surface morphology and molecular dynamic simulations, Polym. Bull. 77 (2019) 3577–3601.
[5] M. Djenane, S. Chafaa, N. Chafai, R. Kerkour, A. Hellal, Synthesis, spectral properties and corrosion inhibition efficiency of new ethyl hydrogen [(methoxyphenyl) (methylamino) methyl] phosphonate derivatives: experimental and theoretical investigation, J. Mol. Struct. 1175 (2019) 398–413.
[6] R. Hsissou, S. Abbout, R. Seghiri, M. Rehioui, A. Berisha, H. Erramli, M. Assouag, A. Elharfi, Evaluation of corrosion inhibition performance of phosphorus polymer for carbon steel in [1 M] HCl: computational studies (DFT, MC and MD simulations), J. Mater. Res. Technol. 9 (2020) 2691–2703.
[7] A. Hammouch, D. Dermaj, P. Chebabe, N. Decaro, N. Hajjaji, H. Bettach, Takenouti, A. Srhiri, Opuntia Ficus indica seed oil: characterization and application in corrosion inhibition of carbon steel in acid medium, Anal. Bioanal. Electrochem 5 (2013) 236–254.
[8] A. Dehghani, G. Bahlakeh, B. Ramezanzadeh, M. Ramezanzadeh, Potential of Borage flower aqueous extract as an environmentally sustainable corrosion inhibitor for acid corrosion of mild steel: electrochemical and theoretical studies, J. Mol. Liq. 277 (2019) 895–911.
[9] M. Zouarhi, S. Abbout, B. Benzidia, M. Chellouli, H. Hammouch, H. Erramli, S.O.S. Hassane, N. Bettach, N. Hajjaji, Evaluation of a new formulation derived from Aleurites moluccana seeds oil as a green corrosion inhibitor for iron in acidic medium, Anal. Bioanal. Electrochem. 11 (2019) 1651–1668.
[10] M. Chellouli, D. Chebabe, A. Dermaj, H. Erramli, N. Bettach, N. Hajjaji, M.P. Casaletto, C. Cirrincione, A. Privitera, A. Srhiri, Corrosion inhibition of iron in acidic solution by a green formulation derived from Nigella sativa L. Electrochim. Acta 204 (2016) 50–59.
[11] P.L. Pérez de Paz, I. Medina Medina, Catálogo de las plantas medicinales de la floracanaria, Aplicaciones populares Instituto de Estudios Canarios, La Laguna, Spain, 1988.
[12] P. Pérez de Paz, C. Hernández Padrón, Plantas medicinales o útiles en la floracanaria, Aplicaciones Populares Francisco Lemus, La Laguna, Spain, 1999.
[13] ISO 659-1988 (E), International Organization for Standardization, 1988.
[14] Recueil des normes Françaises des corps gras, graines oléagineuses, produits dérivés Edité par l'AFNOR, 1984.
[15] N. Hajjaji, N. Bettach, H. Hammouch, A. Srhiri, A. Dermaj, D. Chebabe. OMPIC Casablanca, Morocco. Patent N°3069/10.2011.
[16] K. Rahmouni, S. Joiret, L. Robbiola, A. Srhiri, H. Takenouti, V. Vivier, Corrosion and protection of high leaded tin bronze covered with patina in $NaHCO_3 + Na_2SO_4$ solution simulating acid rain urban environment, Impedance Commun. Line 2 (2004) 5.
[17] M.A. Amin, Weight loss, polarization, electrochemical impedance spectroscopy, SEM and EDS studies of the corrosion inhibition of copper in aerated NaCl solutions, J. Appl. Electrochem. 36 (2006) 215–226.
[18] N.K. Gupta, C. Verma, M.A. Quraishi, A.K. Mukherjee, Schiff's bases derived from l-lysine and aromatic aldehydes as green corrosion inhibitors for mild steel: experimental and theoretical studies, J. Mol. Liq. 215 (2016) 47–57.
[19] G. Cui, J. Guo, Y. Zhang, Q. Zhao, S. Fu, T. Han, S. Zhang, Chitosan oligosaccharide derivatives as green corrosion inhibitors for P110 steel in a carbon dioxide-saturated chloride solution, Carbohydr. Polym. 203 (2019) 386–395.
[20] FAO/WHO Codex Alimentarius Commission, Codex Alimentarius Commission, & Joint FAO/WHO Food Standards Programme. Codex Alimentarius: Fats, Oils and Related Products, 2001, 8.
[21] Z. Ghazi, Contribution à la Valorisation de deux espèces de Cactus de la région d'Oujda : *Opuntia ficus indica* et *Opuntia dillenii*. Evaluation de leurs Activités Antioxydante et Anticorrosive, Doctoral dissertation, Mohammed first University, Oujda, Morocco, 2015.
[22] Z. Ghazi, M. Ramdani, M.L. Fauconnier, B. El Mahi, R. Cheikh, Fatty acids sterols and vitamin E composition of seed oil of Opuntia Ficus indica and Opuntia dillenii from Morocco, J. Mater. Environ. Sci. 4 (2013) 967–972.
[23] A.J.A. Alsaad, A. B Altemimi, S.N. Aziz, N. Lakhssassi, Extraction and identification of cactus *Opuntia dillenii* seed oil and its added value for human health benefits, Pharm. J. 11 (2019) 579–587.
[24] W. Liu, Y.J. Fu, Y.G. Zu, M.H. Tong, N. Wu, X.L. Liu, S. Zhang, Supercritical carbon dioxide extraction of seed oil from *Opuntia dillenii* Haw. and its antioxidant activity, Food Chem. 114 (2009) 334–339.
[25] N. Moussaoui, D. Zerouali, N. Bettahar, Inhibitive effect of date extract on the corrosion of carbon steel in acidic media, J. Chil. Chem. Soc. 61 (2016) 3018–3024.
[26] M. Zouarhi, M. Chellouli, S. Abbout, H. Hammouch, A. Dermaj, S.O. Said Hassane, P. Decaro, N. Bettach, N. Hajjaji, A. Srhiri, Inhibiting effect of a green corrosion inhibitor containing Jatropha curcas seeds oil for iron in an acidic medium, Port. Electrochim. Acta 36 (2018) 179–195.
[27] J.R. Davis, Corrosion: Understanding the Basics, ASM International, 2000.

[28] Z. Tang, A review of corrosion inhibitors for rust preventative fluids, Curr. Opin. Solid State Mater. Sci. 23 (2019) 100759–100775.
[29] S. Frolenkova, T. Overchenko, T. Motronyuk, V. Vorobyova, I. Miroshnychenko, M. Panchenko, Passivating anions effect on the anodic behavior of steel in a converting acetate solution, J. Chem. Techn. Metallu. 54 (2019) 443–446.
[30] M. Chellouli, N. Bettach, N. Hajjaji, A. Srhiri, P. Decaro, Application of a formulation based on oil extracted from the seeds of *Nigella sativa* L., inhibition of corrosion of iron in 3% NaCl, Int. J. Eng. Res. Technol. 3 (2014) 2489–2495.
[31] T. Szauer, A. Brandt, On the role of fatty acid in adsorption and corrosion inhibition of iron by amine- fatty acid salts in acidic solution, Electrochim. Acta 26 (1981) 1219–1224.
[32] A. Khanra, M. Srivastava, M.P. Rai, R. Prakash, Application of unsaturated fatty acid molecules derived from microalgae toward mild steel corrosion inhibition in HCl solution: a novel approach for metal–inhibitor association, ACS Omega 3 (2018) 12369–12382.
[33] A. Ehsani, M.G. Mahjani, M. Hosseini, R. Safari, R. Moshrefi, H.M. Shiri, Evaluation of Thymus vulgaris plant extract as an eco-friendly corrosion inhibitor for stainless steel 304 in acidic solution by means of electrochemical impedance spectroscopy, electrochemical noise analysis and density functional theory, J. Colloid Interface Sci. 490 (2017) 444–451.
[34] S. Abbout, M. Chellouli, M. Zouarhi, B. Benzidia, H. Hammouch, D. Chebabe, A. Dermaj, H. Erramli, N. Bettach, N. Hajjaji, New formulation based on *ceratonia siliqua L* seed oil, as a green corrosion inhibitor of iron in acidic medium, Anal. Bioanal. Electrochem. 10 (2018) 789–804.
[35] M. Damej, D. Chebabe, M. Benmessaoud, A. Dermaj, H. Erramli, N. Hajjaji, A. Srhiri, Corrosion inhibition of brass in 3% NaCl solution by 3-methyl-1,2,4-triazol-5-thione, Corros. Emng. Sci. Technol. 50 (2015) 103–107.
[36] H.H. Zhang, C.K. Qin, Y. Chen, Z. Zhang, Inhibition behaviour of mild steel by three new benzaldehyde thiosemicarbazone derivatives in 0.5 M H_2SO_4: experimental and computational study, R. Soc. Open Sci. 6 (2019) 190192–190211.
[37] S.J. Seo, H. Jeon, J.K. Lee, G.Y. Kim, D. Park, H. Nojima, J. Lee, S.H. Moon, Investigation on removal of hardness ions by capacitive deionization (CDI) for water softening applications, Water Res. 44 (2010) 2267–2275.
[38] H. Liu, D. Xu, A.Q. Dao, G. Zhang, Y. Lv, H. Liu, Study of corrosion behavior and mechanism of carbon steel in the presence of Chlorella vulgaris, Corrosion Sci. 101 (2015) 84–93.
[39] J.P. Diard, B. Le Gorrec, C. Montella, Linear diffusion impedance. General expression and applications, J. Electroanal. Chem. 471 (1999) 126–131.
[40] K. Benchekroun, F. Dalard, J.J. Rameau, A. El Ghazali, Inhibition de la corrosion du fer dans HCL 1 M. Partie II. Etude des propriétés inhibitrices du 2-aminothiophénol et du 2-aminophényl disulfure, par spectroscopie d'impédance, New J. Chem. 26 (2002) 946–952.
[41] L.T. Popoola, Organic green corrosion inhibitors (OGCIs): a critical review, Corrosion Rev. 37 (2018) 71–102.